Electronic supplementary information

Nickel Nanograins Anchoring on Carbon Framework for Efficient Hydrogen Evolution Electrocatalyst and Flexible Electrode

Zhiwei Zhang[a], Linjie Deng[b], Zhe Zhao[a], Yuting Zhao[a], Jingyu Yang[a], Jun Jiang[b,*], Gaoshan Huang[a,*] and Yongfeng Mei[a]

[a] Department of Materials Science, Fudan University, Shanghai 200433, China

[b] Hefei National Laboratory for Physical Sciences at the Microscale, School of Chemistry and Materials Science, University of Science and Technology of China, Hefei 230026, China

* Corresponding authours.

E-mail address: jiangj1@ustc.edu.cn. (J. Jiang), gshuang@fudan.edu.cn. (G. S. Huang).

Supplementary videos:

Video 1 shows the HER process of Co-NCF@600-Ni/CFP on 30-mm-diameter Teflon rod in 1 M KOH. The flexible catalyst belt was used as working electrode directly. During the process, it can be clearly observed that abundunt H_2 bubbles were generated upon the catalyst region while no gas was produced on the bare CFP.

Video 2 shows the details of one rolling cycle of Co-NCF@600-Ni/CFP on 30-mm-diameter rod. After every 10 rolling cycles, the belt was tested for the HER performance. The same one belt was used throughout the experiment.

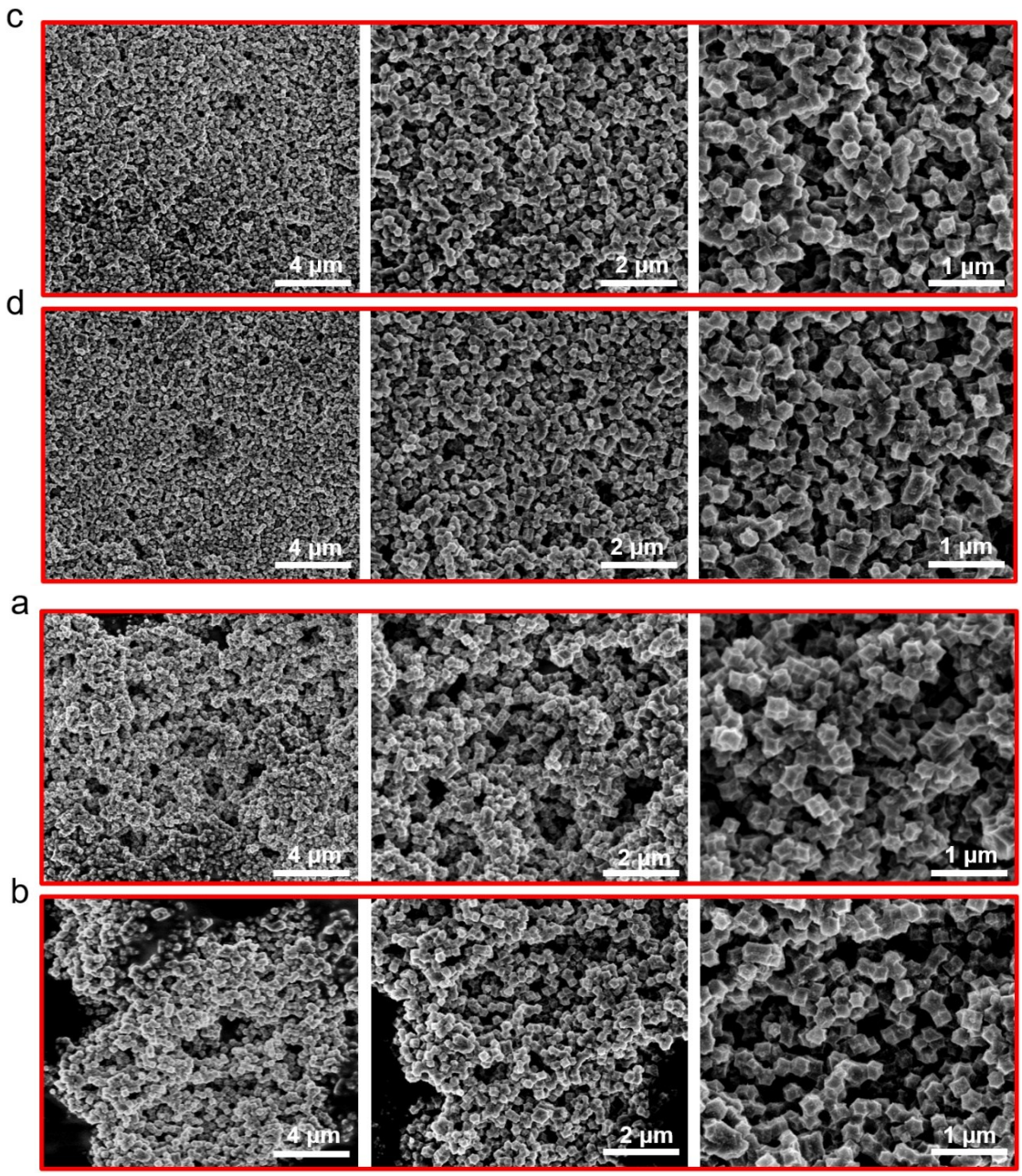
c
4 μm
2 μm
1 μm
d
4 μm
2 μm
1 μm
a
4 μm
2 μm
1 μm
b
4 μm
2 μm
1 μm

Fig. S1 FESEM images of a) Co-NCF, b) Co-NCF@100-Ni, c) Co-NCF@400-Ni, and d) Co-NCF@600-Ni.

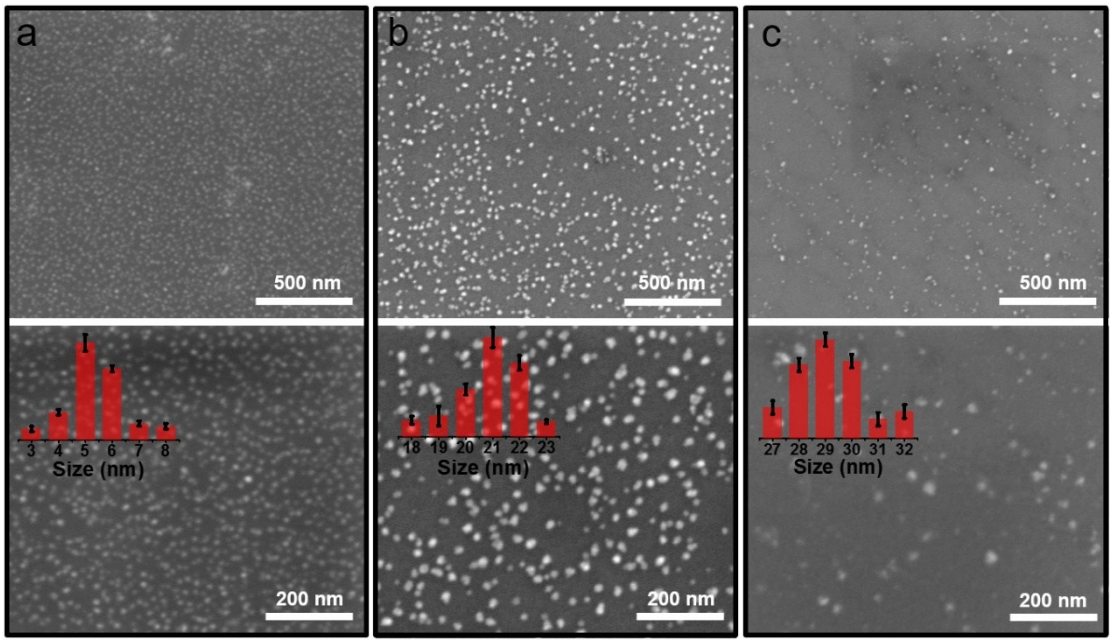

Fig. S2 FESEM images of a) 100 cycles Ni, b) 400 cycles Ni, and c) 600 cycles Ni deposited on silicon wafers.

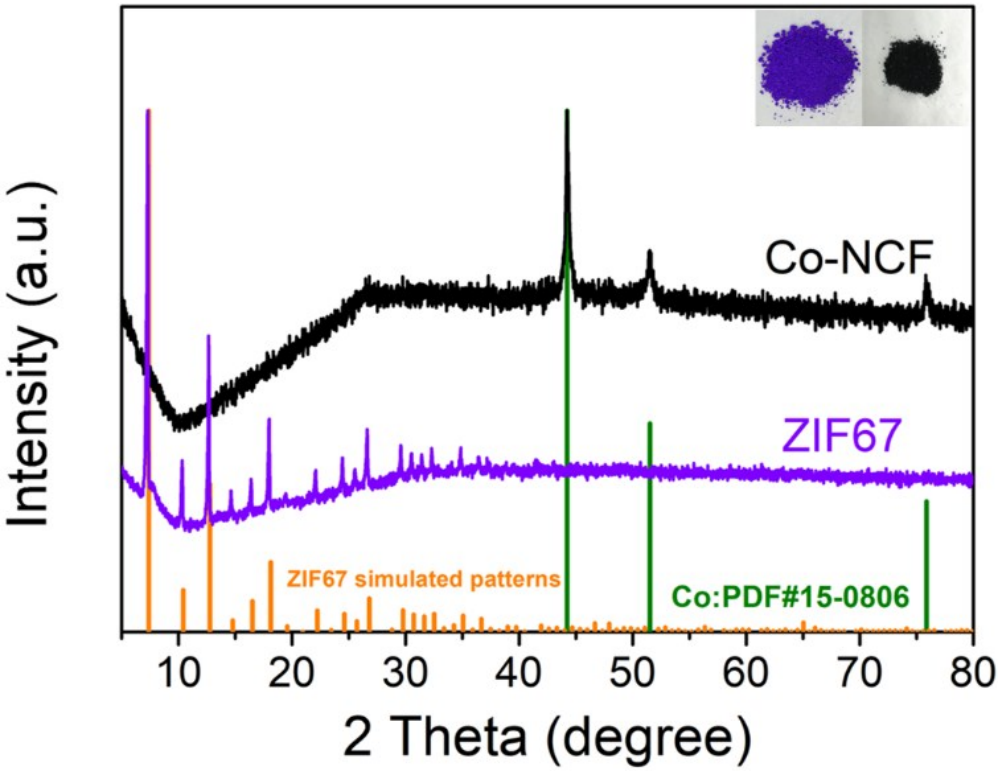

Fig. S3 XRD patterns of ZIF-67 and Co-NCF (Left inset: digital photo of ZIF-67 sample. Right inset: digital photo of Co-NCF sample).

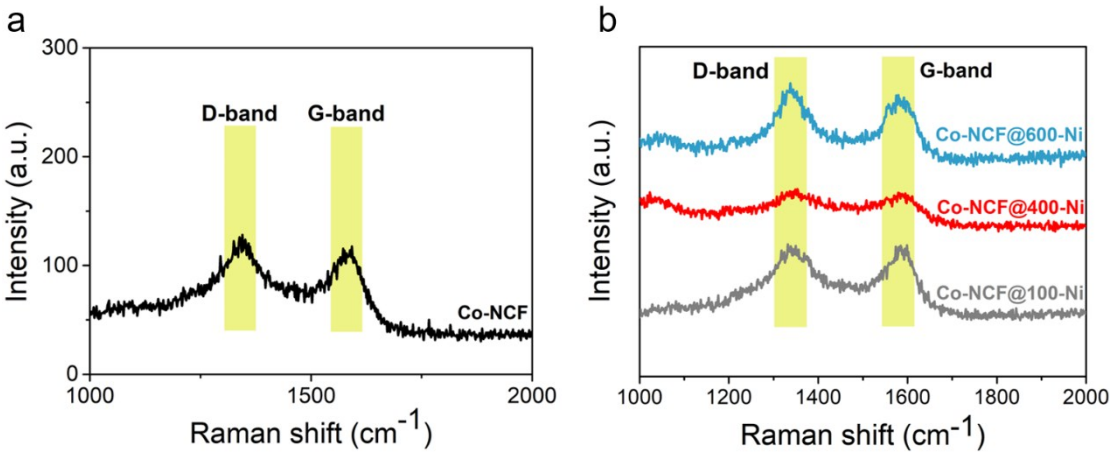

Fig. S4 (a) Raman spectrum of Co-NCF. (b) Raman spectra of Co-NCF@100-Ni, Co-NCF@400-Ni, and Co-NCF@600-Ni.

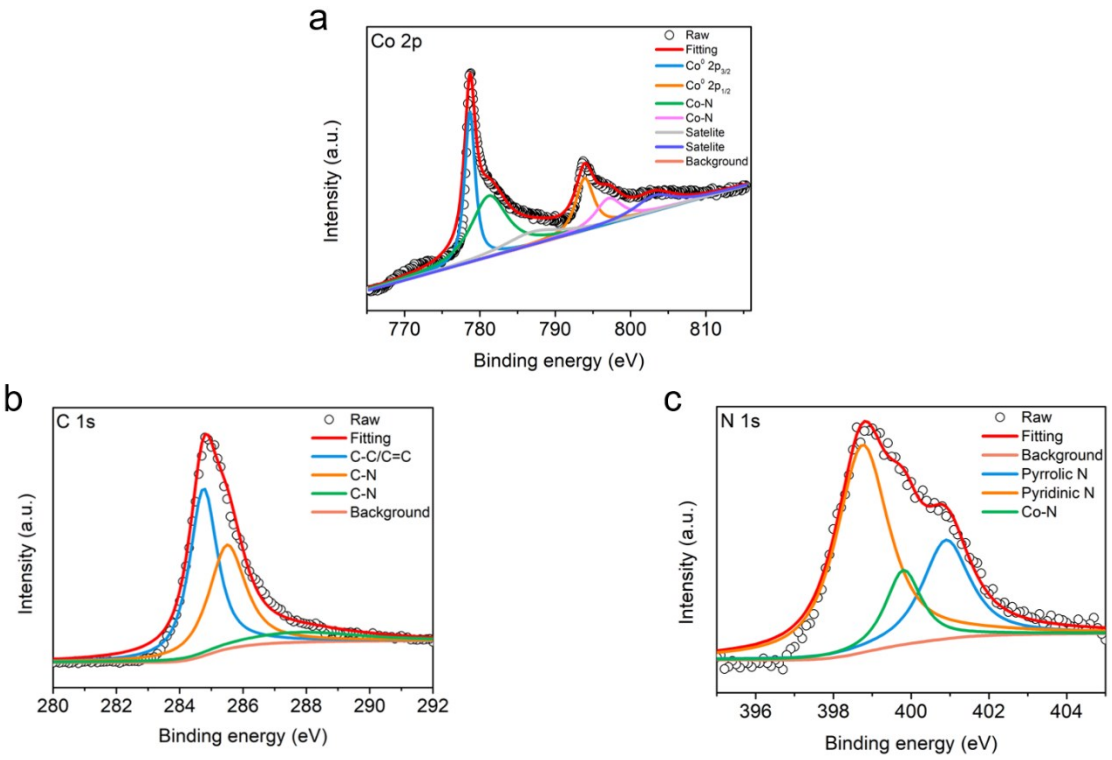

Fig. S5 High-resolution (a) Co 2p, (b) C 1s, and (c) N 1s XPS spectra of Co-NCF.

Two peaks at 778.6 (Co $2p_{3/2}$) and 793.8 eV (Co $2p_{1/2}$) in Fig. S7a suggest the presence of metallic Co which indicate the fully reduction of cobalt ions after the pyrolysis. The peaks at 781.2 and 784.7 eV in Fig. S5a are assigned to the Co-N bonds which have been proved as efficient active sites for HER processes in some reported works.[1,2] The peaks of C-C bonds (284.8 eV) and C-N bonds (285.5 and 287.7 eV) shown in high-resolution C 1s spectrum (Fig. S5b) and the peaks of Pyrrolic N (400.9 eV), Pyridinic N (398.8 eV), and Co-N bonds (399.8 eV) shown in high-resolution N 1s spectrum (Fig. S5c) reveal the elemental compositions and states of the Co-NCF.

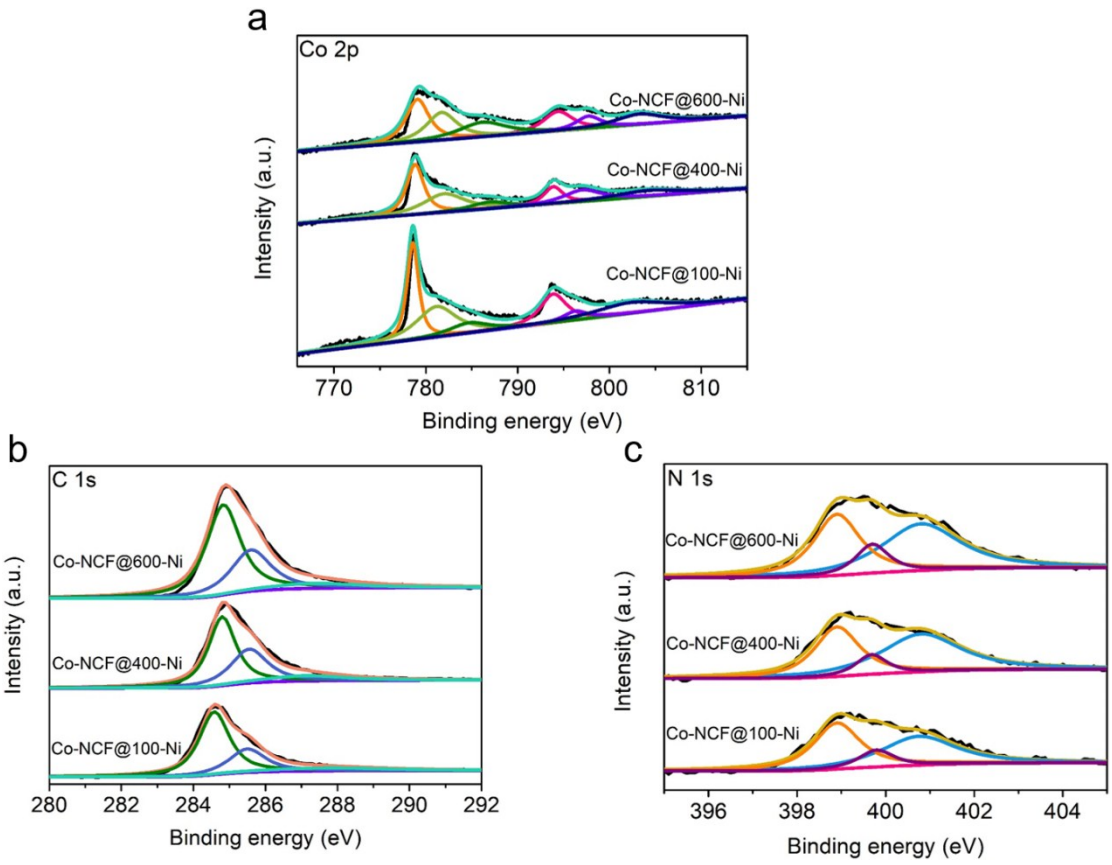

Fig. S6 a) High-resolution (a) Co 2p, (b) C 1s, and (c) N 1s XPS spectra of Co-NCF@100-Ni, Co-NCF@400-Ni, and Co-NCF@600-Ni.

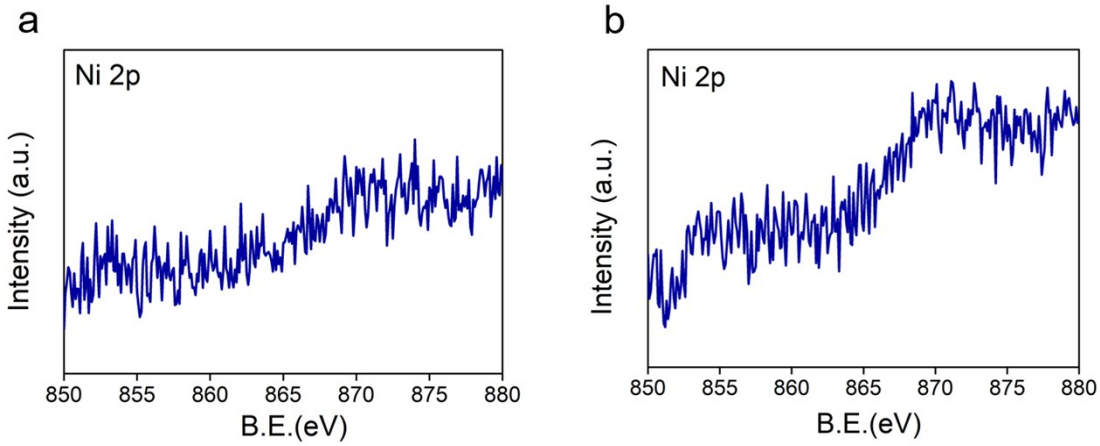

Fig. S7 Ni 2p XPS spectrum of (a) Co-NCF@100-Ni and (b) Co-NCF@400-Ni.

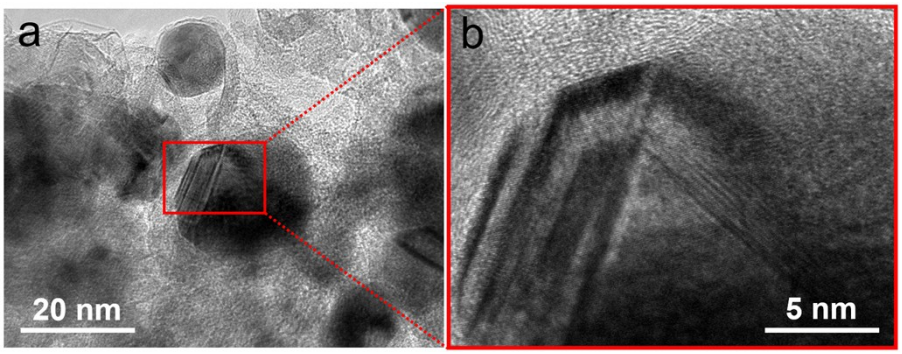

Fig. S8 (a, b) HRTEM images of Co-NCF@600-Ni.

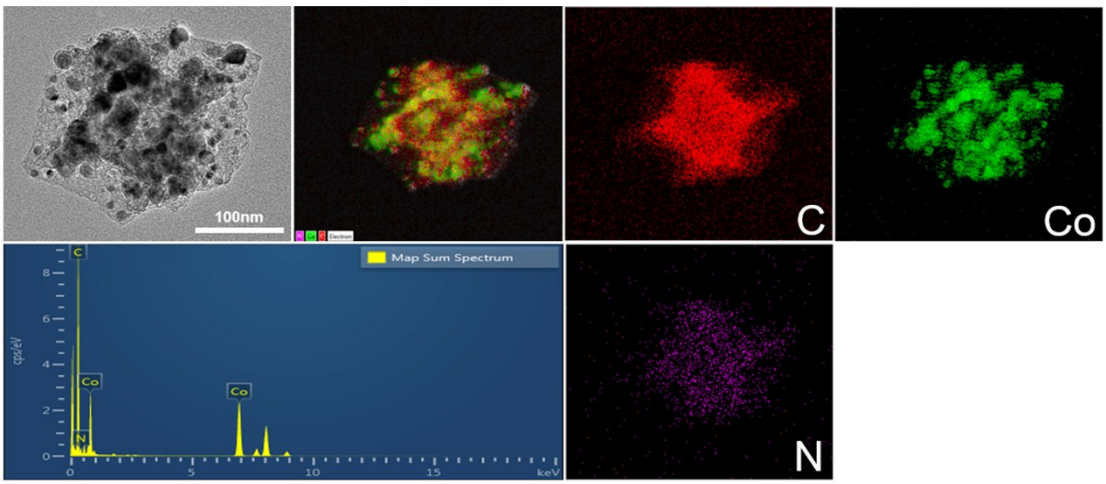

Element	Line Type	Wt%	Atomic %
C	K series	74.66	92.34
N	K series	1.57	1.66
Co	K series	23.78	5.99
Total:		100.00	100.00

Fig. S9 EDX mapping results of Co-NCF showing the presence of C, N, and Co.

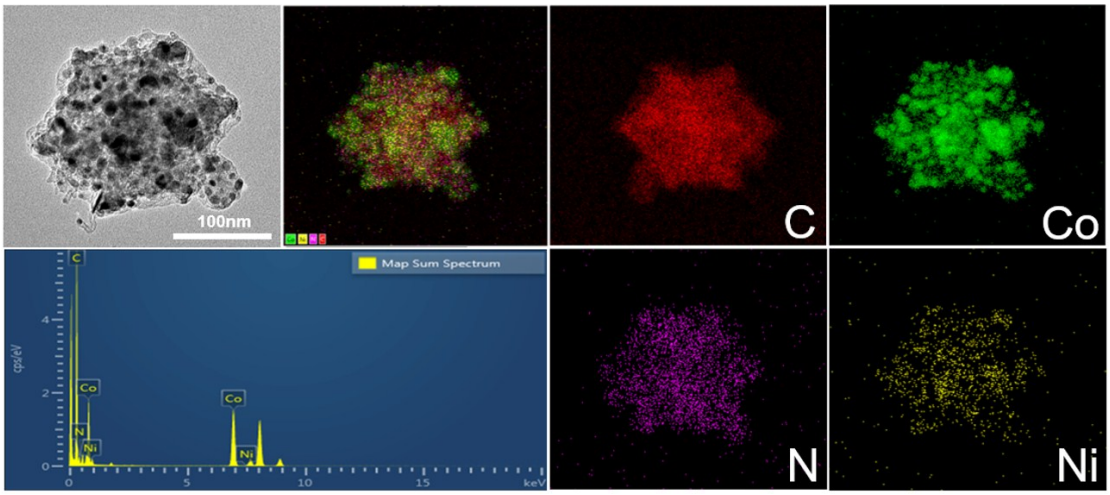

Element	Line Type	Wt%	Atomic %
C	K series	72.70	91.10
N	K series	2.35	2.53
Co	K series	19.78	5.05
Ni	K series	5.16	1.32
Total:		100.00	100.00

Fig. S10 EDX mapping results of Co-NCF@100-Ni showing the presence of C, N, Co, and Ni.

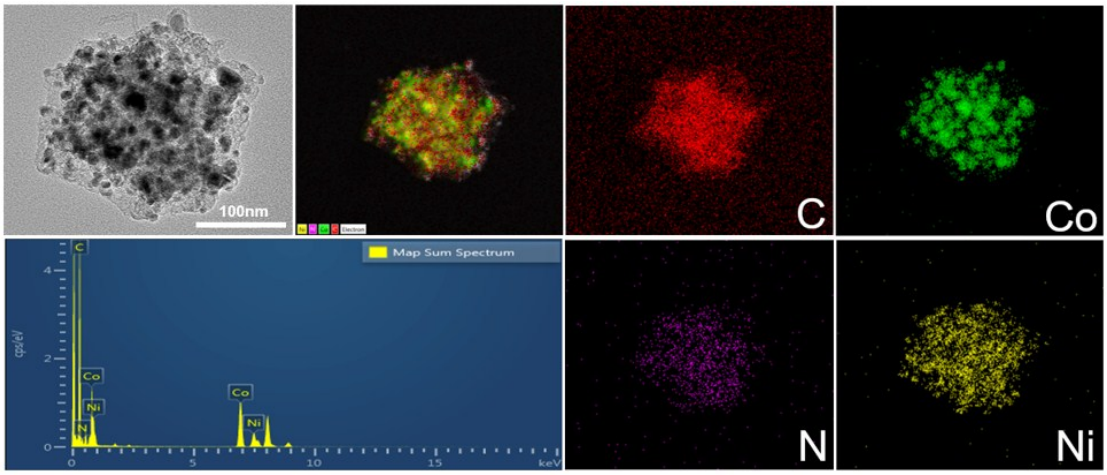

Element	Line Type	Wt%	Atomic %
C	K series	58.88	84.95
N	K series	3.12	3.86
Co	K series	24.89	7.32
Ni	K series	13.11	3.87
Total:		100.00	100.00

Fig. S11 EDX mapping results of Co-NCF@400-Ni showing the presence of C, N, Co, and Ni.

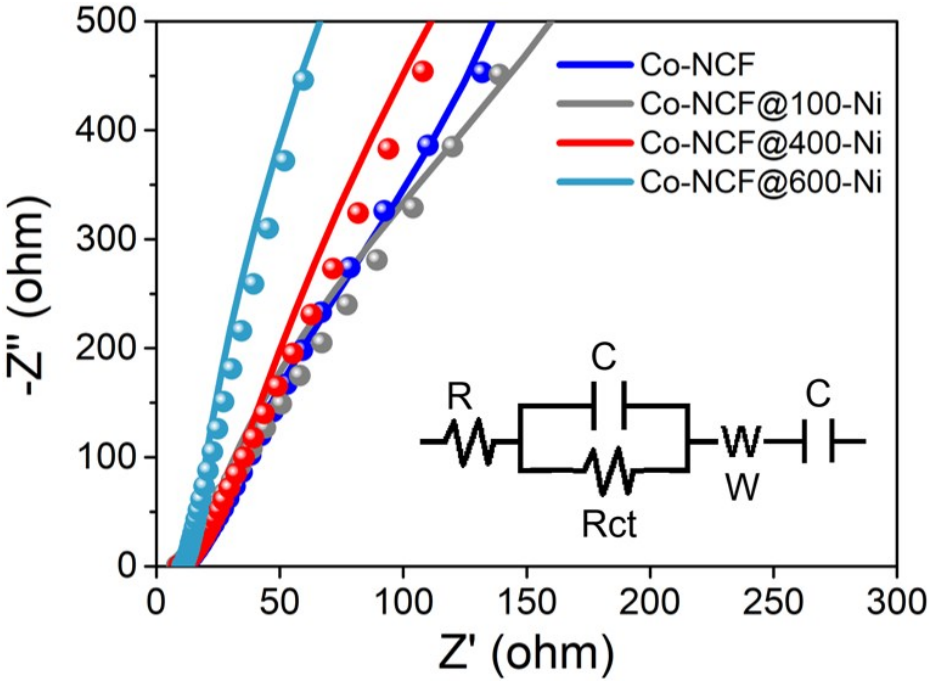

	Co-NCF	Co-NCF@100-Ni	Co-NCF@400-Ni	Co-NCF@600-Ni
R	1.031×10 Ω	7.838×10 Ω	9.196×10 Ω	1.035×10 Ω
C	2.653×10^{-4} F	1.261×10^{-4} F	4.623×10^{-4} F	9.029×10^{-4} F
Rct	1.117×10^{2} Ω	1.993×10^{2}Ω	2.562×10^{3} Ω	2.909×10^{2} Ω
W	2.591×10^{-3} Ω^{-1} $s^{0.5}$	2.222×10^{-3} Ω^{-1} $s^{0.5}$	2.894×10^{-3} Ω^{-1} $s^{0.5}$	1.137×10^{-2} Ω^{-1} $s^{0.5}$
C	1.013×10^{-4} F	7.324×10^{-5} F	1.581×10^{-4} F	2.574×10^{-4} F

Fig. S12 EIS spectra and fitted curves of Co-NCF, Co-NCF@100-Ni, Co-NCF@400-Ni, and Co-NCF@600-Ni electrodes.

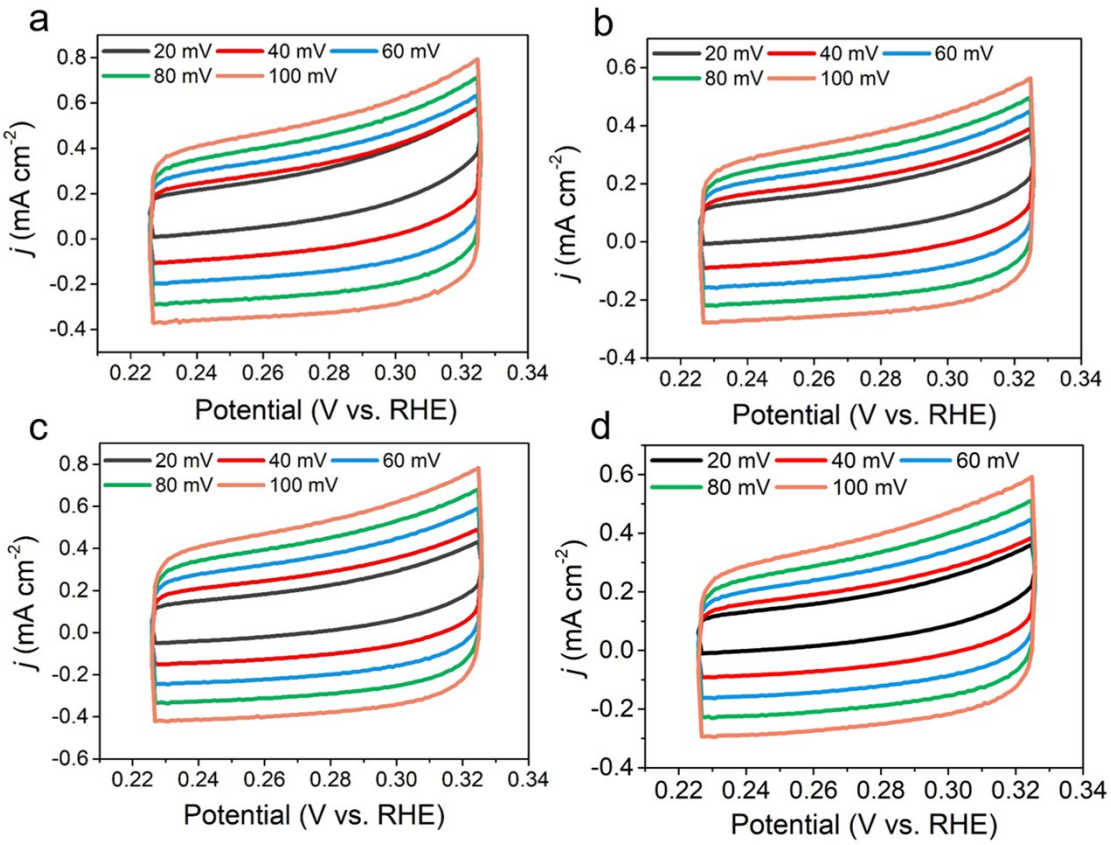

Fig. S13 CV curves at different scan rates of a) Co-NCF catalyst, b) Co-NCF@100-Ni catalyst, c) Co-NCF@400-Ni catalyst, and d) Co-NCF@600-Ni catalysts.

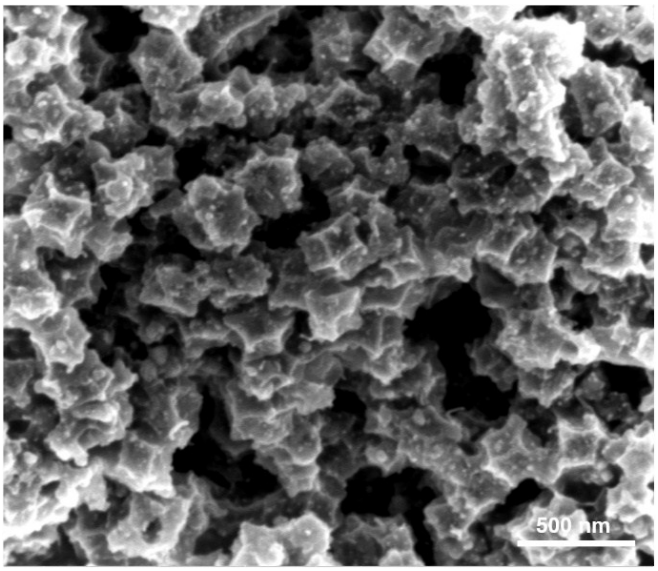

Fig. S14 SEM image of Co-NCF@600-Ni after 20 h chronoamperometric test.

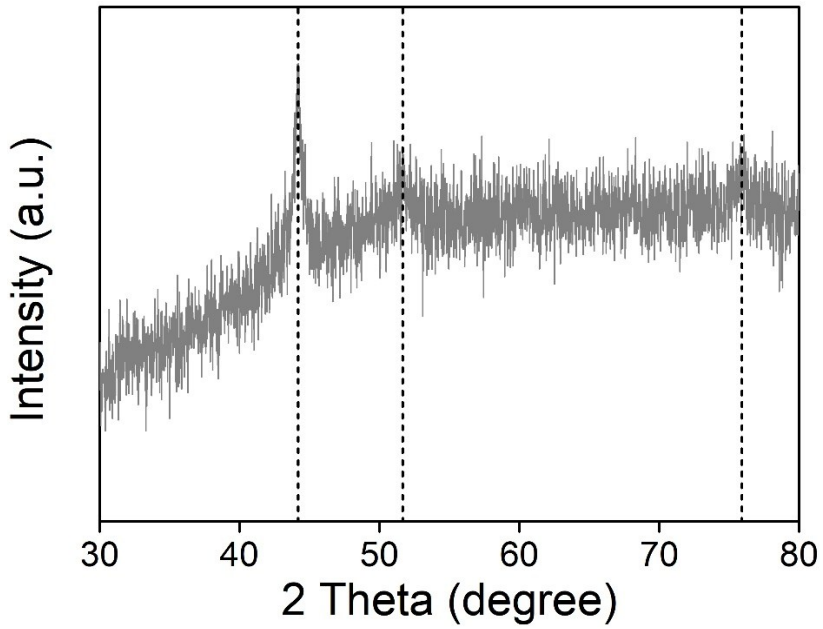

Fig. S15 XRD pattern of Co-NCF@600-Ni after 20 h chronoamperometric test.

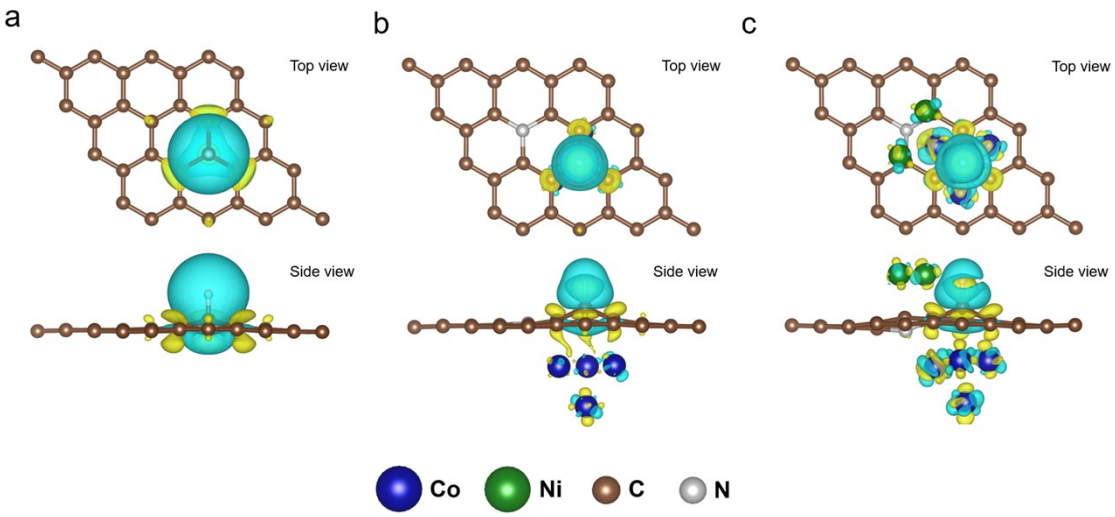

Fig. S16 The difference charge density of H adsorbed on three different systems: (a) C-H system, (b) Co@NC-H system, and (c) Co@NC@Ni (2:1) system. The blue, green, brown, and silver, balls represent Co, Ni, C, and N atoms, respectively. The blue and yellow isosurfaces show the electron losing and gaining, respectively.

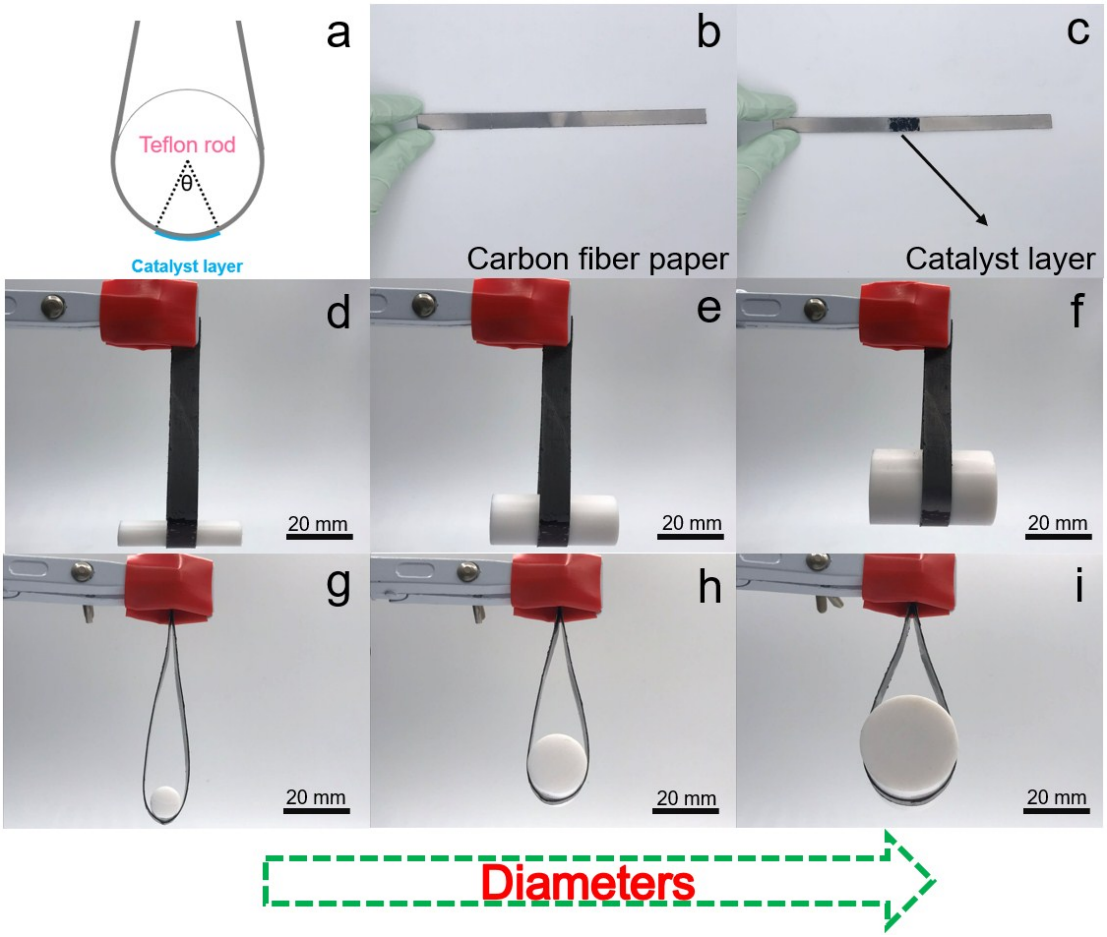

Fig. S17 (a) Schematic illustration of the structure of Co-NCF@600-Ni/CFP electrode. Digital photos of (b) CFP and c) Co-NCF@600-Ni/CFP belt. (d-f) Front view photos and (g-i) lateral view photos of Co-NCF@600-Ni/CFP rolling onto (d, g) 10-mm Teflon rod, (e, h) 20-mm Teflon rod, and (f, i) 30-mm Teflon rod.

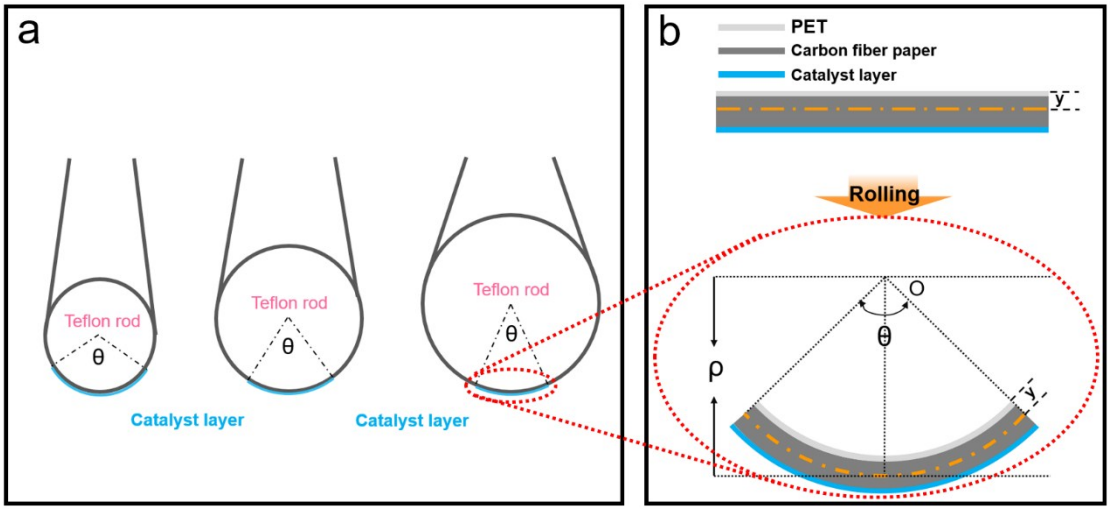

Fig. S18 Schematic illustration of the structure of (a) Co-NCF@600-Ni/CFP belt rolling onto 10-mm, 20-mm and 30-mm rods and (b) the enlarged details of the rolled catalytic region of Co-NCF@600-Ni/CFP belt.

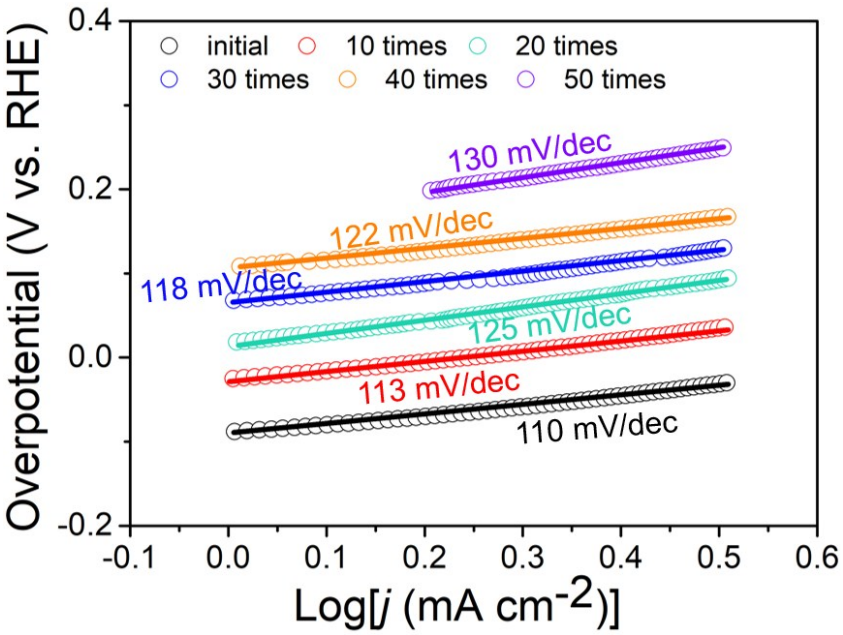

Fig. S19 Tafel curves of Co-NCF@600-Ni on 30-mm-diameter rod after different rolling times.

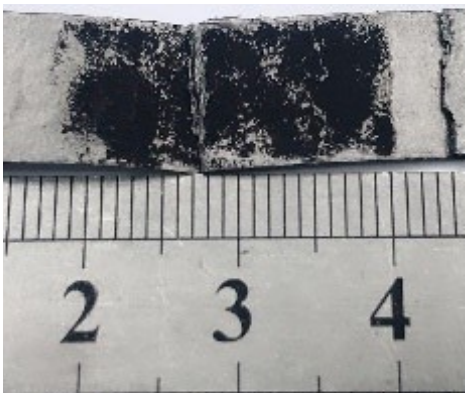

Fig. S20 Digital photo of the Co-NCF@Ni/CFP electrode after 50 times of rolling and several times of electrochemical tests.

Table S1. Elemental content of Co-NCF@600-Ni according to EDX spectrum.

Element	Line Type	Wt%	Atomic %
C	K series	60.35	85.56
N	K series	3.19	3.88
Co	K series	17.65	5.10
Ni	K series	18.80	5.45
Total:		100.00	100.00

Table S2. Geometry and mechanical parameters of Co-NCF@600-Ni/CFP rolling onto 10-mm rod, 20-mm rod and 30-mm rod.

	R = 10 mm	**R = 20 mm**	**R = 30 mm**
Radius	$\rho = 10.4$ mm	$\rho = 20.4$ mm	$\rho = 30.4$ mm
Radian	$\theta \approx 3.846$ rad	$\theta \approx 1.961$ rad	$\theta \approx 1.316$ rad
Strain	$\varepsilon \approx 0.0192$	$\varepsilon \approx 0.0098$	$\varepsilon \approx 0.0066$

References

[1] J. P. Lai, B. L. Huang, Y. G. Chao, X. Chen and S. J. Guo, Adv. Mater., 2019, **31**, 1805541.

[2] H. Tang, S. Cai, S. Xie, Z. Wang, Y. Tong, M. Pan and X. Lu, Adv. Sci., 2016, **3**, 1500265.